Advanced Materials & Sustainable Manufacturing

SCIEPublish

Article

Achieving High Strength and Ductility of Ti_2AlNb Alloy Fabricated by Electron Beam Powder Bed Fusion

Zhihao Zhu [1,*], Ping Liu [2] and Liang Jia [1,3]

[1] State Key Laboratory of Porous Metal Materials, Northwest Institute for Non-Ferrous Metal Research, Xi'an 710016, China; jialiang_nin@126.com (L.J.)
[2] School of Materials Science and Engineering, Xi'an University of Technology, Xi'an 710074, China; liuping18709@163.com (P.L.)
[3] Industry Engineering Department, School of Mechanical Engineering, Northwestern Polytechnical University, Xi'an 710072, China

* Corresponding author. E-mail: zhuzhihaonin@163.com (Z.Z.)

Received: 17 September 2026; Revised: 8 October 2026; Accepted: 27 October 2026; Available online: 6 November 2026

ABSTRACT: Ti_2AlNb alloy is a promising lightweight high-temperature structural material for aerospace. In this study, Ti_2AlNb alloys were fabricated by electron beam powder bed fusion (EB-PBF) using pre-alloyed Ti-22Al-25Nb (at,%) powders. This work optimizes the substrate preheating temperature and scanning speed of the EB-PBF process to achieve superior strength. The microstructure, tensile properties, and crack propagation mechanism of the as-deposited alloy were systematically studied. The EB-PBFed Ti_2AlNb alloy exhibits a typical refined basket-weave microstructure with uniformly fine lamellar O-phases and dispersed remnant B2 laths. The alloy achieves favorable strength-ductility synergy both at room temperature (ultimate tensile strength (UTS) of 1178 ± 10 MPa, yield strength (YS) of 1058 ± 7 MPa and elongation of 3 ± 0.6%) and at 650 °C (UTS of 933 ± 12 MPa, YS of 790 ± 5 MPa and elongation of 4 ± 1%). Fracture analysis indicates that boundaries of coarse primary O-phases are the main sites for crack initiation and propagation due to local stress concentration and dislocation tangling. The optimized process contributes to retarding the precipitation of coarse primary O-phases and restrains crack evolution, enabling simultaneous improvement of strength and ductility. This work provides an effective route to obtain high strength and ductility in EB-PBF-fabricated Ti_2AlNb alloy for aerospace high-temperature lightweight components.

Keywords: Ti_2AlNb alloy; Electron beam powder bed fusion; Microstructure; Mechanical properties

1. Introduction

Ti_2AlNb alloys is a key candidate for aerospace high-temperature lightweight components due to their unique comprehensive advantages of low density, excellent high-temperature strength, fracture toughness, and creep resistance [1–3]. The alloy exhibit great potential to replace high-density nickel-based superalloys for aerospace hot-end parts, such as compressor casings, turbine disks, and nozzle components [2].

Compared with conventional γ-TiAl alloys, the addition of 13–30 at.% Nb element optimizes the phase composition and microstructure of titanium aluminide alloys, effectively improving their intrinsic room-

© 2026 The authors. This is an open access article under the Creative Commons Attribution 4.0 International License (https://creativecommons.org/licenses/by/4.0/).

temperature brittleness and crack propagation resistance [4,5]. Conventional manufacturing technologies for Ti_2AlNb alloys, including precision casting [6] and forging [7], face prominent technical bottlenecks. In traditional manufacturing, the inherent narrow thermal processing window and poor room-temperature formability of Ti_2AlNb alloy led to complex processing procedures, high production costs, and low material utilization rate [8–10]. Moreover, it is difficult for conventional processes to fabricate integrated complex structural components, which severely limits the large-scale engineering application of Ti_2AlNb alloy in high-precision and complex aerospace parts. Additive manufacturing fabricates parts via layer-by-layer material deposition guided by digital models, enabling near-net-shape production of complex structural components and greatly reducing manufacturing cycles and material waste for intermetallic alloys [9]. As a mature and advanced metal additive manufacturing technology, Electron beam powder bed fusion (EB-PBF) [9,10] adopts a high-energy electron beam as the heat source and operates under a high-vacuum and high preheating temperature environment. Relative to the widely used laser powder bed fusion (L-PBF), EB-PBF features lower residual stress, slower cooling rate, and lower cracking susceptibility, which can effectively avoid typical defects such as thermal cracking and porosity in the forming process of brittle intermetallic alloys [11]. This unique process advantage makes EB-PBF extremely suitable for the near-net-shape forming of difficult-to-process Ti_2AlNb alloy components with complex geometries.

Nevertheless, EB-PBF-fabricated Ti_2AlNb alloys still suffer from a prominent strength-ductility trade-off, which is the key constraint restricting their engineering popularization. Due to the rapid layer-by-layer melting and solidification of additive manufacturing, as well as the unique high-temperature thermal cycle of EB-PBF, the as-built Ti_2AlNb alloy usually presents heterogeneous microstructures including primary B2 columnar grains, coarse primary O phases, fine secondary O precipitates, and oriented Widmanstätten laths [12]. The non-equilibrium microstructure induced by rapid solidification often endows the alloy with high tensile strength but extremely low room-temperature ductility; conversely, optimizing process parameters to improve ductility will inevitably lead to the deterioration of strength performance [13,14]. In addition, process-induced microstructural anisotropy, irregular grain morphology, and residual microdefects further exacerbate the imbalance between strength and ductility, making it difficult to obtain coordinated high strength and high ductility in as-built EB-PBF Ti_2AlNb alloys. At present, most existing studies [15–18] mainly focus on the influence of a single process parameter or post-heat treatment on the microstructure and mechanical properties of as-deposited Ti_2AlNb alloys. The internal correlation mechanism between process regulation, phase transformation behavior, and strength-ductility synergy is still unclear. There is still a lack of systematic strategies and in-depth mechanism research to break the strength-ductility trade-off and achieve balanced comprehensive mechanical properties.

Therefore, this study focuses on the microstructure regulation and strength-ductility synergy optimization of the Ti_2AlNb alloy by optimizing the substrate preheating temperature and scanning speed of the EB-PBF process. The microstructure, mechanical properties, and crack propagation mechanism of the as-fabricated alloys are clarified. This work provides theoretical support and a technical reference for the engineering application of high-strength, high-ductility Ti_2AlNb alloy in advanced aerospace high-temperature lightweight structural parts.

2. Materials and Methods

Spherical pre-alloyed Ti-22Al-25Nb (at.%) powder was used as the raw material for fabricating Ti_2AlNb alloys via electron beam powder bed fusion (EB-PBF). The powder was produced by plasma rotating electrode atomization (PREA), supplied by Xi'an Sailong Additive Manufacturing Technology Co., Ltd., Xi'an, China, with a particle size range of 45–150 μm (average: 80 μm [12]), and its chemical composition, measured using inductively coupled plasma atomic emission spectrometry (ICP-AES) is 22.58 at.% Al, 24.66 at.% Nb, 0.22 at.% O, 0.02 at.% N, 0.03 at.% H, with Ti as the balance [12]. The morphology of the as-received pre-alloyed powder is shown in Figure 1. Ti_2AlNb specimens were

additively manufactured using a commercial EB-PBF system (Sailong-Y150, Xi'an Sailong Additive Manufacturing Technology Co., Ltd., Xi'an, China). The EB-PBF processing parameters were kept constant throughout fabrication: an acceleration voltage of 60 kV, a beam current of 8 mA, a focused beam diameter of 300 μm, a layer thickness of 50 μm, a scanning speed of 3.2 m/s, and a hatch distance of 100 μm. A layer-wise scanning rotation of 90° was adopted to reduce microstructural anisotropy in the as-built alloys. Before printing, a 316L stainless steel substrate was preheated to 940 °C to alleviate residual thermal stress and eliminate solidification-induced defects. The substrate preheating temperature was raised from 830 °C, as reported in ref. [11], to 940 °C in the present study. This higher preheating temperature suppresses powder blowing and reduces thermal gradients across the deposited layers, thereby mitigating thermal stress and restraining crack initiation. The scanning speed was decreased from 3.6 m/s [12] to 3.2 m/s, which extends local thermal exposure and promotes adequate B2→O phase transformation to generate fine lamellar O-phases. Bulk Ti_2AlNb alloy blocks with dimensions of 90 mm × 30 mm × 30 mm were fabricated layer-by-layer under a high-purity helium atmosphere. The density of EB-PBF-fabricated Ti_2AlNb bulk samples, measured using an XS64 electronic densimeter, is 5.34 g/cm^3, which is close to the theoretical density of 5.4 g/cm^3. In our previous work, X-ray CT was employed on similar EB-PBFed Ti_2AlNb samples, revealing that the total volume fraction of pores is approximately 0.87% [12]. These results confirm that high-quality Ti_2AlNb components can be fabricated via the EB-PBF process.

Microstructural features of the as-built Ti_2AlNb samples were observed by scanning electron microscopy (SEM, JSM-IT510, JEOL Ltd., Tokyo, Japan), and phase constituents were identified by X-ray diffraction (XRD, Bruker D8, Bruker AXS, Karlsruhe, Germany) with Cu Kα radiation. Electron backscatter diffraction (EBSD) was performed on an SEM5000 system with a step size of 0.05 μm, and the acquired datasets were processed using AztecCrystal software (Version 2.1, Oxford Instruments, High Wycombe, UK). The thickness and volume fraction of the orthorhombic O-phase were measured statistically from multiple SEM micrographs using ImageJ software (Version 1.47, National Institutes of Health, Bethesda, MD, USA) to ensure the accuracy and statistical reliability of the microstructural data. For tensile testing, standard cylindrical specimens with a gauge length of 25 mm and a gauge diameter of 5 mm were machined from the bulk alloy blocks in accordance with Chinese national standards. Uniaxial tensile tests were conducted on an electronic universal testing machine (Instron 5985, Instron Corporation, Norwood, MA, USA) at a quasi-static constant strain rate of $1 \times 10^{-3} \cdot s^{-1}$. A static extensometer (MFHT5, MF Mess-& Feinwerktechnik GmbH, Velbert, Germany) was attached to the specimen gauge section to precisely acquire real-time strain data during loading. Two duplicate specimens were tested for each processing condition to minimize experimental deviation and verify the repeatability of mechanical results. It is noteworthy that only two tensile specimens were tested for each condition in the present work, which imposes certain limitations on the statistical evaluation of mechanical properties.

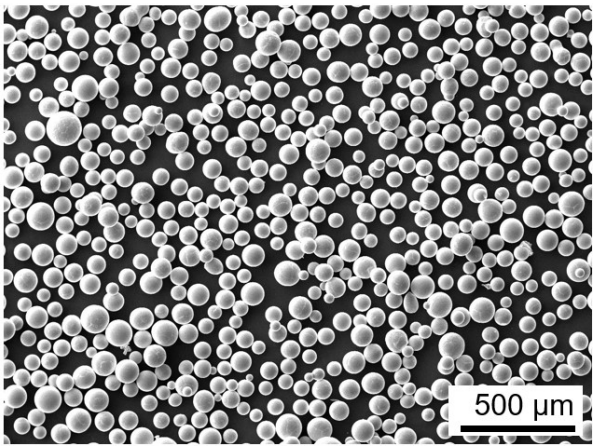


Figure 1. SEM micrograph showing Ti_2AlNb powders.

3. Results and Discussion

3.1. Microstructure

Figure 2a–c presents SEM micrographs of the EB-PBFed Ti_2AlNb alloy. As shown in Figure 2a, the microstructure is dominated by the B2 matrix, with coarse, plate-like primary O phases preferentially precipitating along B2 grain boundaries and forming a discontinuous grain-boundary network. The grain size distribution is presented in Figure 2d; the statistically averaged grain size is 152 μm. At higher magnification (Figure 2b,c), the EB-PBFed Ti_2AlNb alloy exhibits a typical basket-weave microstructure consisting of alternating fine lamellar O phases and residual white B2 laths. Abundant fine lamellar secondary O phases appear in the B2 matrix, as shown in Figure 2c. These intragranular secondary O laths possess a uniform submicron width. The coexistence of grain-boundary primary O phases and intragranular secondary O phases constitutes the duplex microstructure of the present Ti_2AlNb alloy. The thickness and volume fraction of O and B2 phases are listed in Table 1. The average thickness of fine secondary O precipitates is approximately 0.08 μm. The volume fraction of the remnant B2 phase is ~44%. The XRD pattern of the as-deposited Ti_2AlNb alloy (Figure 3) identifies diffraction peaks corresponding to the ordered B2 matrix and orthorhombic O phase.

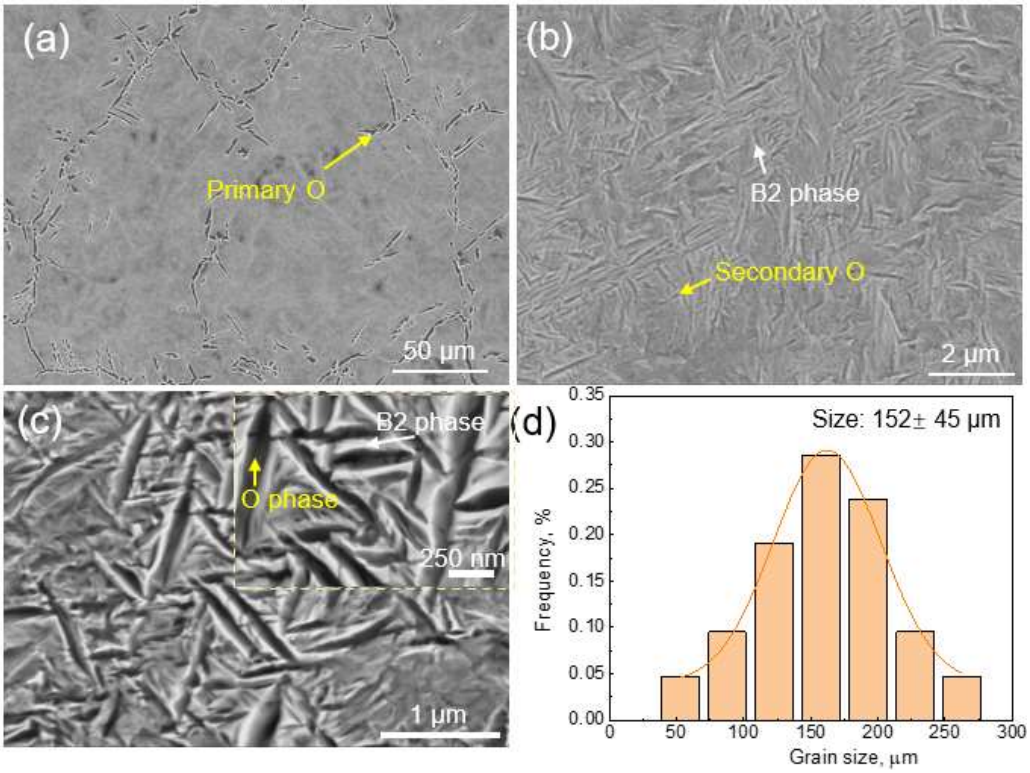


Figure 2. SEM images of primary O phases and fine secondary O phases in the B2 matrix (**a**–**c**), and grain size distribution histogram (**d**) for the as-deposited Ti_2AlNb alloy.

Table 1. Thickness and volume fraction of O and B2 phases.

Parameter	Microstructure Characters		
	Primary O	**Secondary O**	**B2**
Thickness (μm)	2.6 ± 0.3	0.08 ± 0.01	-
Volume fraction (%)	8.7 ± 1.1	47.3 ± 1.6	44 ± 1.5

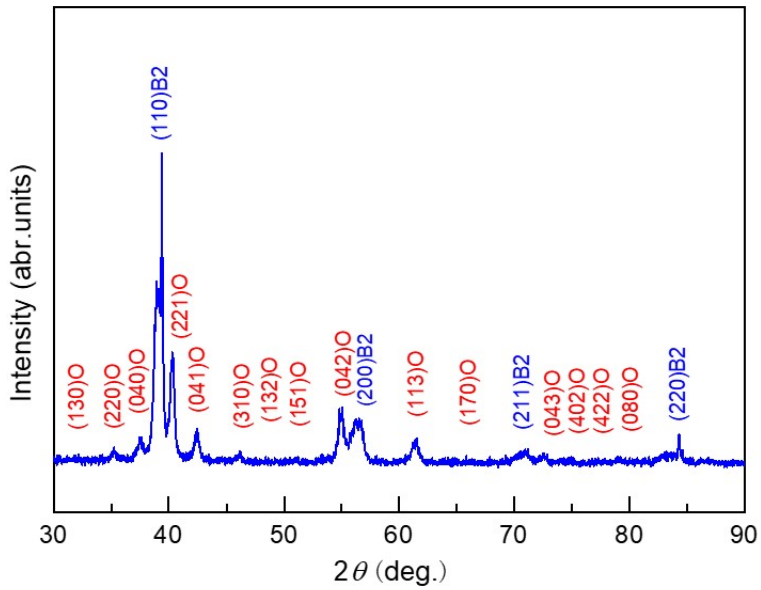


Figure 3. XRD pattern of as-deposited Ti_2AlNb alloy.

3.2. Mechanical Properties

Figure 4 presents the tensile performance of as-deposited Ti_2AlNb alloy at room temperature (25 °C) and at 650 °C. As shown in Figure 4a, the room-temperature ultimate tensile strength (UTS) and yield strength (YS) reach 1178 ± 10 MPa and 1058 ± 7 MPa, with an elongation of 3 ± 0.6%. The samples show reasonable stress-strain reproducibility with small standard deviations. In previously reported EB-PBF-fabricated Ti_2AlNb alloys, the UTS ranges from 989 to 1159 MPa [11,12,16]. By employing a newly developed electron beam printing strategy, the present Ti_2AlNb alloy attains a superior tensile strength of 1178 MPa. This high strength originates from the reduced volume fraction of coarse O-phases, together with the combined strengthening effect of the B2 matrix and finely dispersed O-phase precipitates. The volume fraction of residual coarse O-phases is approximately 8.7%, which is substantially lower than the 12–26% reported in the literature [5,11,12]. The decreased fraction of primary coarse O-phases and the formation of abundant fine lamellar O-phases account for the strength enhancement.

At 650 °C, the as-deposited Ti_2AlNb alloy maintains a high UTS of 933 ± 12 MPa, YS of 790 ± 5 MPa, and elongation of 4 ± 1%. The UTS decreases from 1178 MPa at room temperature to 933 MPa at 650 °C, corresponding to approximately 80% strength retention. At elevated temperatures, thermally induced softening of the B2 matrix and partial stress relaxation around O-phase precipitates activate more dislocation slip systems and promote plastic flow [19,20]. This reveals distinctly different active deformation mechanisms compared with room-temperature loading. The corresponding strain-hardening rate curves are plotted in Figure 4b. The samples exhibit a continuous drop in the strain-hardening rate with increasing true strain, which is governed by the competition between dislocation multiplication and dynamic recovery. Generally, deformation mechanisms are active at elevated temperatures. The 650 °C specimen displays a more rapid decay of the strain-hardening rate and a lower minimum hardening rate, which arises from accelerated dynamic recovery under high-temperature conditions.

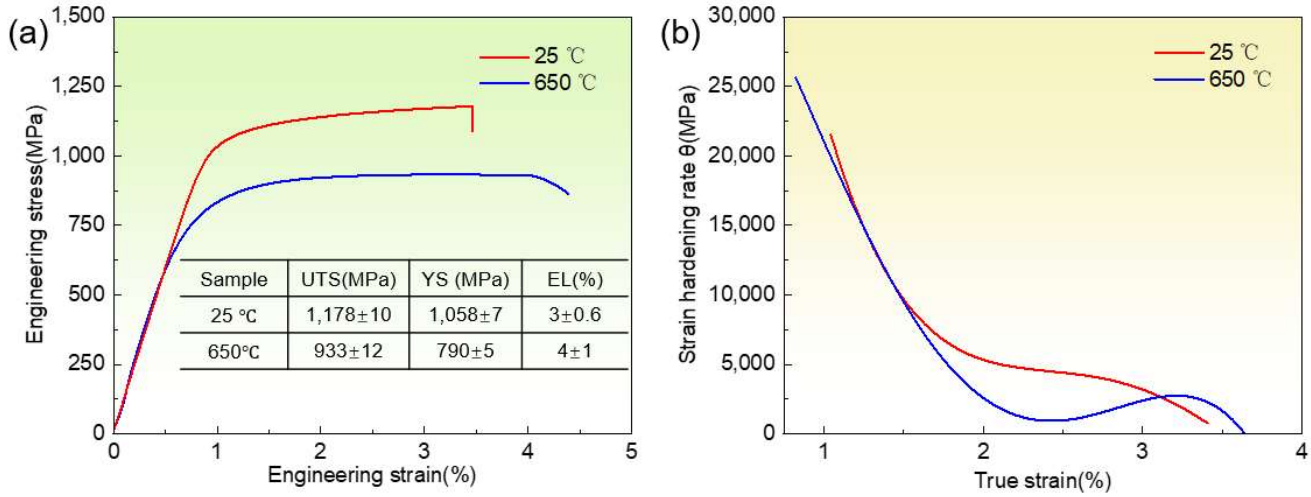


Figure 4. Mechanical properties of the as-deposited Ti_2AlNb alloy: (**a**) Engineering tensile stress-stain curves; (**b**) Strain-hardening rate curves.

Figure 5 shows a comparison of tensile properties of Ti_2AlNb alloys at 650 °C between the present alloy and previously reported counterparts [2] fabricated via various manufacturing routes, including EB-PBF, L-PBF, powder metallurgy (PM), and conventional forging. The EB-PBFed Ti_2AlNb alloy developed in this work exhibits a balanced combination of tensile strengths and ductility. At 650 °C, its ultimate tensile strength and elongation are superior to those reported for other EB-PBFed Ti_2AlNb alloys. By contrast, PM and L-PBFed Ti_2AlNb alloys show much lower tensile strength than the current alloy. The present as-deposited Ti_2AlNb alloy achieves tensile strengths even comparable to those of conventional forged Ti_2AlNb alloys.

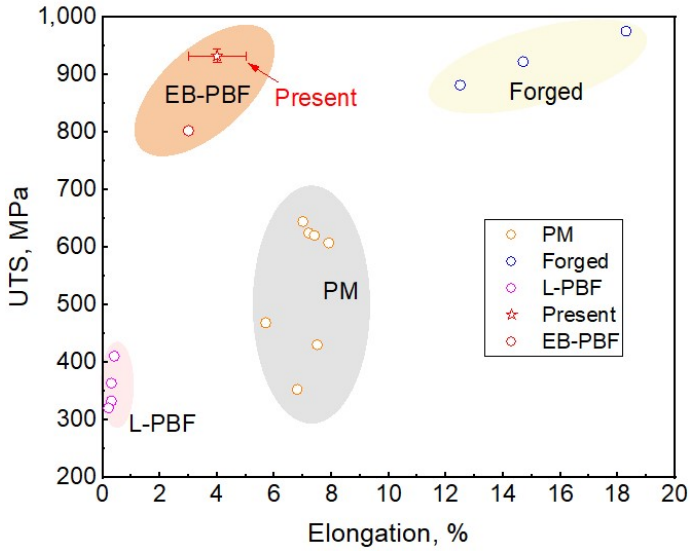


Figure 5. Comparison of the tensile properties between the present and reported Ti_2AlNb alloys [2] at 650 °C. Note: PM, L-PBF, and EB-PBF denote powder metallurgy, Electron beam powder bed fusion, and laser powder bed fusion, respectively.

Figure 6 shows SEM images of as-deposited Ti_2AlNb alloy after tensile tests at 25 °C and 650 °C. At room temperature (Figure 6a–c), fracture surfaces are dominated by cleavage steps and numerous microcracks, with only sparse dimples and tear ridges, manifesting a typical quasi-brittle fracture behavior. The pre-existing microcracks and brittle O-phase precipitates within the B2 matrix readily act as crack initiation sites under room-temperature loading, which promotes rapid crack propagation and results in low tensile elongation. For samples tensile at 650 °C (Figure 6d–f), the fraction of dimples and tear-ridge structures obviously increases.

Residual unmelted powder particles and microcracks originating from additive manufacturing defects are still visible on the fracture surface. Elevated temperature activates dislocation slip and alleviates local stress concentration around brittle O-phase, facilitating local plastic deformation [21]. Nevertheless, cleavage facets are not completely eliminated, suggesting a mixed quasi-cleavage-ductile fracture mode. This micro-fracture feature well accounts for the enhanced ductility at 650 °C.

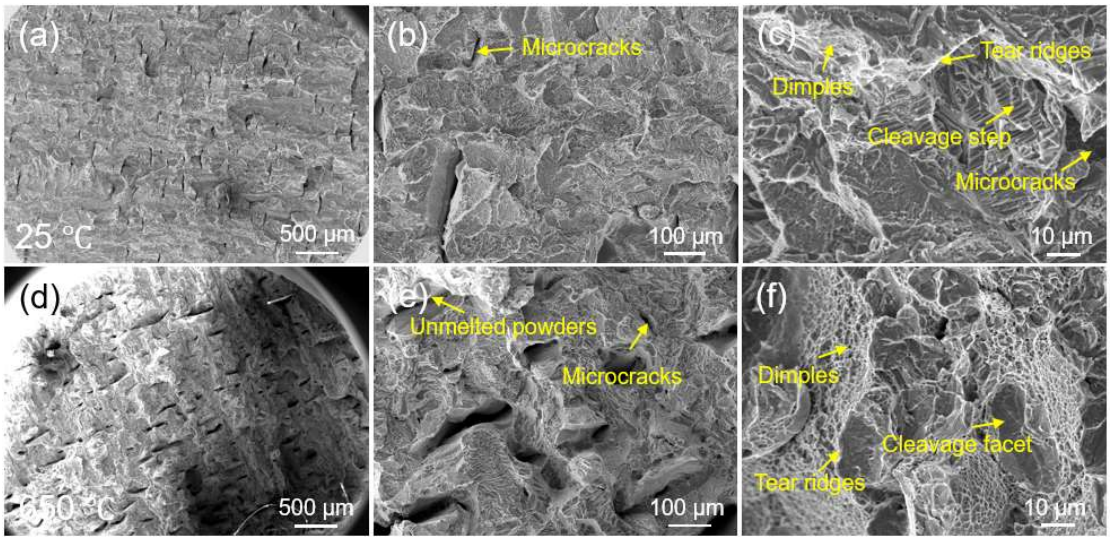


Figure 6. SEM images of near-fracture surfaces fracture surfaces for the as-deposited Ti_2AlNb alloy tensile tests at (**a**–**c**) 25 °C, and (**d**–**f**) 650 °C.

Figure 7 shows the cross-sectional SEM observations near the fracture tip of as-deposited Ti_2AlNb alloy after tensile deformation at 25 °C and 650 °C. At room temperature (Figure 7a–c), microcracks preferentially nucleate within or at the interfaces of coarse primary O-phase laths. The brittle primary O-phase possesses limited dislocation accommodating capacity [22], high local stress concentrates at O/B2 phase boundaries under external loading, which triggers crack initiation. Once these microcracks are formed, they propagate rapidly along O-phase laths or phase interfaces, accelerating final fracture and accounting for the low room-temperature ductility. For specimens tested at 650 °C (Figure 7d–f), microcrack nucleation is still associated with coarse primary O phase. Nevertheless, elevated temperature enables local dislocation relaxation at phase boundaries and relieves peak stress concentration [20]. Although crack initiation cannot be fully suppressed, the crack propagation rate is retarded to some extent, which contributes to the improved tensile elongation at 650 °C. In both temperature conditions, coarse primary O laths serve as intrinsic crack-initiation sites for the as-deposited dual-phase microstructure.

Figure 8 presents multi-scale characterizations of the fracture tip of the EB-PBFed Ti_2AlNb alloy after tensile testing at 650 °C. Figure 8a shows the macroscopic morphology of two broken tensile specimens, where fracture occurs within the gauge section. The yellow box marks the region selected for subsequent EBSD observation at the fracture tip. From the inverse pole figure (IPF) map (Figure 8b, a continuous microcrack propagates along the phase boundaries. The phase map (Figure 8c) demonstrates that the microcrack preferentially nucleates and extends along the interfaces between the coarse B2 matrix and lamellar O phases. The kernel average misorientation (KAM) map (Figure 8d) displays elevated local misorientation/strain concentration adjacent to the microcrack path, indicating that strain accumulates at the B2/O phase interfaces under high-temperature tensile loading. These interfaces act as the preferential sites for crack initiation and propagation at 650 °C. As evidenced by these EBSD results, though complete suppression of crack initiation is unattainable, the crack growth is moderately reduced at elevated temperature, contributing to the enhanced tensile elongation observed in Figure 4a. Notably, this work only focuses on short-term tensile performance at 650 °C; however, the creep performance and long-term

thermal stability critical for aerospace structural applications have not been quantified. Follow-up creep and long-term thermal exposure studies are thus required to validate the high-temperature durability of EB-PBF-fabricated Ti_2AlNb alloys.

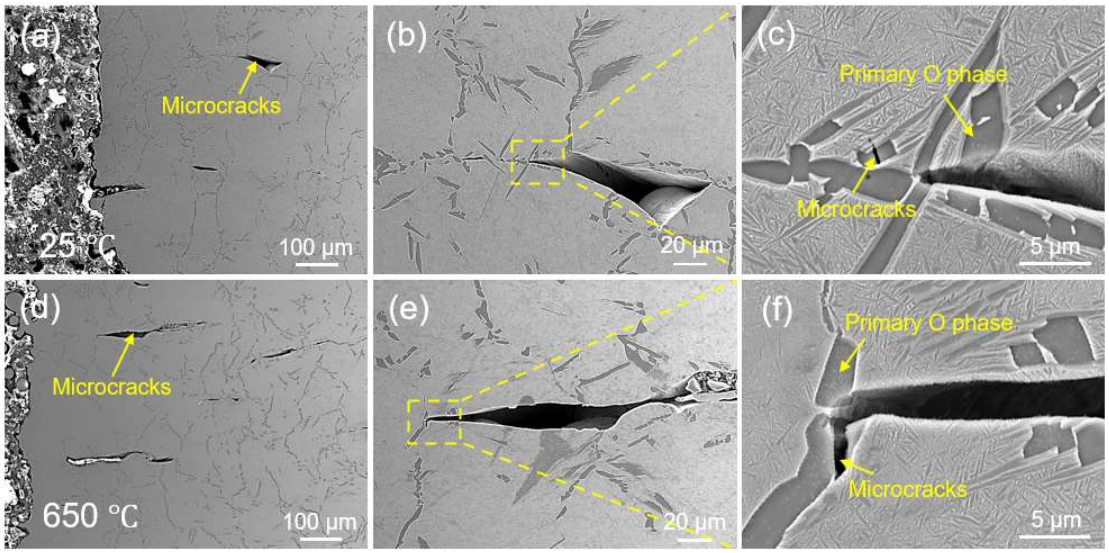


Figure 7. SEM image of fracture surfaces for the as-deposited Ti_2AlNb alloys tensile tests at (**a**–**c**) 25 °C, and (**d**–**f**) 650 °C.

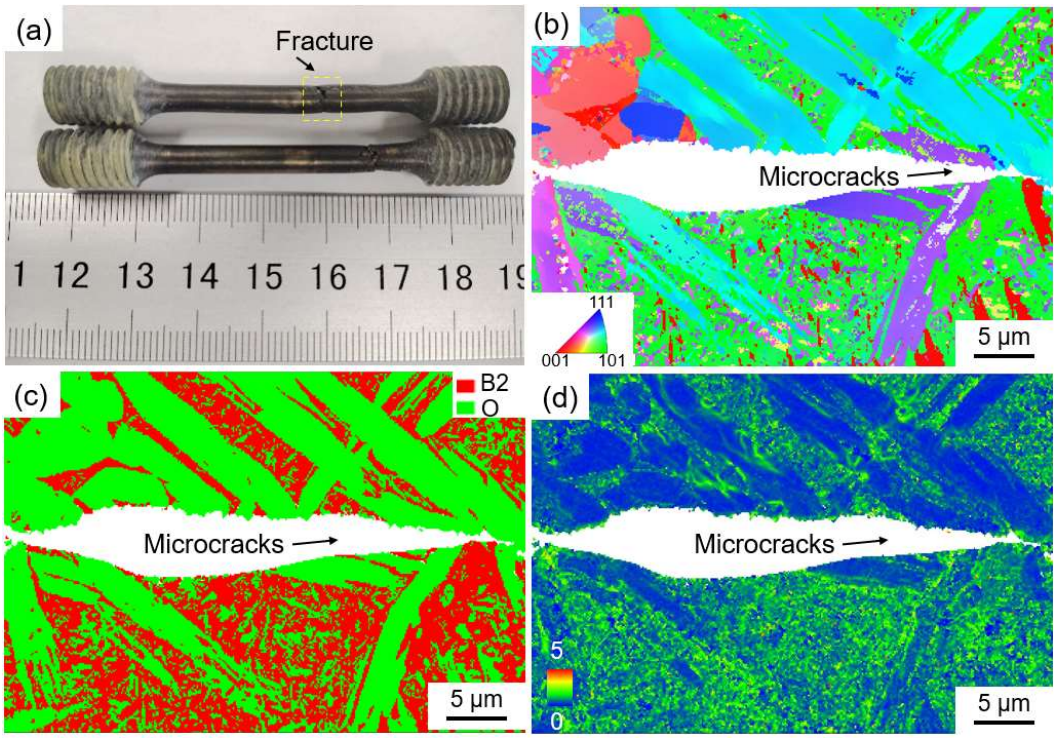


Figure 8. Characterizations of the fracture tip for the EB-PBFed Ti_2AlNb tensile specimen fractured at 650 °C: (**a**) Macroscopic image of the failed tensile samples, (**b**) IPF map showing microcracks near the fracture tip, (**c**) EBSD phase map (red: B2 phase, green: O phase), (**d**) KAM map revealing local strain distribution around microcracks.

4. Conclusions

In summary, this study investigated the microstructure, mechanical properties, and crack propagation mechanism of the as-deposited Ti_2AlNb alloy. The main conclusions are as follows:

(1) Optimized EB-PBF processing enables the fabrication of Ti_2AlNb alloys with a refined basket-weave microstructure, characterized by uniform fine lamellar O-phases and dispersed residual B2 laths. The

tailored process favors retarding the formation of coarse primary O-phase laths and mitigates microstructural inhomogeneity.

(2) The alloy exhibits balanced strength-ductility synergy at both room and elevated temperatures. It delivers a room-temperature ultimate tensile strength of 1178 ± 10 MPa, yield strength of 1058 ± 7 MPa, and elongation of 3 ± 0.6%, and maintains a high tensile strength of 933 ± 12 MPa and yield strength of 790 ± 5 MPa with an enhanced ductility of 4 ± 1% at 650 °C, verifying the remarkable improvement in mechanical performance via process optimization.

(3) Coarse primary O-phase boundaries act as dominant crack initiation and propagation sites, where stress concentration and drive crack growth. The optimized fabrication process inhibits the precipitation of coarse primary O-phases, restrains crack evolution, and enhances the alloy's mechanical properties.

Acknowledgments

The authors are grateful to Jingzhe Niu for valuable assistance on EBSD characterization.

Author Contributions

Z.Z.: Conceptualization, Investigation, Validation, Writing—original draft, Writing—review & editing, Funding acquisition. P.L.: Resources, Validation, Formal analysis. L.J.: Methodology.

Ethics Statement

Not applicable.

Informed Consent Statement

Not applicable.

Data Availability Statement

Data will be made available on request.

Funding

This work was supported by the National Natural Science Foundation of China (No. 52601036), the Key Research and Development Project of Shaanxi Province (No. 2025CY-YBXM-579, No. 2026CY-YBXM-554, No. 2025CY-GJHX-17), the Research Project of Northwest Institute for Nonferrous Metal Research (No. 0601YK2520).

Declaration of Competing Interest

The authors declare that they have no known competing financial interests or personal relationships that could have appeared to influence the work reported in this paper.

References

1. Hu R, Zhang KW, Zou H, Gao ZT, Luo X, Liu XX, et al. Research progress on Ti_2AlNb-based alloys and composites for aerospace applications. *J. Alloys Compd.* **2025**, *1021*, 179701. DOI:10.1016/j.jallcom.2025.179701
2. Liu P, Zhu ZH, Jia L. Powder-based additive manufacturing of Ti_2AlNb alloys: A review of processes, microstructure and mechanical properties. *High-Temp. Mater.* **2026**, *3*, 10010. DOI:10.70322/htm.2026.10010
3. Xue XY, Bao JG, Wu ZK, Zhao Y, Da RH, Yang DB, et al. Additive manufacturing of Ti_2AlNb alloys: A review of process, microstructure, property relationships. *Mater. Sci. Eng. R Rep.* **2026**, *169*, 101197. DOI:10.1016/j.mser.2026.101197

4. Li QC, Xiao SL, Liang ZQ, Jiang G, Wang YF, Tian Y, et al. Mechanisms governing synergistic enhancement of strength-plasticity and α_2 thermal stability in TiAl alloys fabricated via selective electron beam melting. *Mater. Sci. Eng. A* **2026**, *950*, 149561. DOI:10.1016/j.msea.2025.149561
5. Zhu ZH, Niu JZ, Zhang XZ, Liu N, Jia L, Wang J. Microstructure and mechanical behaviors of the additive-manufactured Ti-22Al-25Nb intermetallic fabricated via selective electron beam melting. *J. Alloys Compd.* **2026**, *1061*, 187481. DOI:10.1016/j.jallcom.2026.187481
6. Chai YP, Zhu YC, Qin L, Luo YY, Niu Y, Shao ZC. High-temperature hot deformation behavior and processing map of Ti-22Al-25Nb alloy. *Mater. Today Commun.* **2024**, *41*, 110599. DOI:10.1016/j.mtcomm.2024.110599
7. Xue C, Zeng WD, Wang W, Liang XB, Li S, Zhang JW. Quantitative analysis on microstructure evolution and tensile property for the isothermally forged Ti_2AlNb based alloy during heat treatment. *Mater. Sci. Eng. A*. **2013**, *573*, 183-189. DOI: 10.1016/j.msea.2013.03.003
8. Zhou YH, Li WP, Wang DW, Zhang L, Ohara K, Shen J, et al. Selective laser melting enabled additive manufacturing of Ti-22Al-25Nb intermetallic: Excellent combination of strength and ductility, and unique microstructural features associated. *Acta Mater.* **2019**, *173*, 117–129. DOI:10.1016/j.actamat.2019.05.008
9. Che QY, He WW, Li HX, Cheng KK, Wang Y. Microstructure and property of Ti_2AlNb alloy by selective electron beam melting. *J. Mater. Eng.* **2022**, *50*, 156–164. DOI:10.11868/j.issn.1001-4381.2021.000958
10. Jiao M, Long H, Xiao B, Liang X, Lin F. Electron beam powder bed fusion additive manufacturing: A comprehensive review and its development in China. *Addit. Manuf. Front.* **2024**, *3*, 200177. DOI:10.1016/j.amf.2024.200177
11. Chen Q, Xu LY, Zhang YK, Zhao L, Hao KD, Ren WJ, et al. Additive manufacturing Ti-22Al-25Nb alloy with excellent high temperature tensile properties by electron beam powder bed fusion. *Addit. Manuf.* **2024**, *86*, 104236. DOI:10.1016/j.addma.2024.104236
12. Zhu ZH, Zhang XZ, Niu JZ, Jia L, Liu N. Microstructure and mechanical properties of the additive-manufactured Ti_2AlNb intermetallic fabricated via electron beam melting. *Intermetallics* **2026**, *195*, 109349. DOI:10.1016/j.intermet.2026.109349
13. Hu JX, Xi X, Chen Q, He ZH, Cong ZR, Li S, et al. Mechanism of O phase induced property variation in Ti_2AlNb alloy via laser powder bed fusion over a wide temperature range. *Mater. Sci. Eng. A* **2026**, *972*, 150609. DOI:10.1016/j.msea.2026.150609
14. Li CJ, Wang XL, Fan B, Wang HJ, Meng Y, Yuan ZP, et al. Process-microstructure-property interplay in LPBF-fabricated Ti-22Al-25Nb alloy. *Mater. Today Commun.* **2026**, *54*, 115481. DOI:10.1016/j.mtcomm.2026.115481
15. Jia Z, Zhang Y, Meng FC, Yu QY, Sun FB, Sun H, et al. Improving the uniform deformation ability and ductility of powder metallurgical Ti_2AlNb intermetallic with single-step solution heat treatment. *J. Alloys Compd.* **2025**, *1011*, 178377. DOI:10.1016/j.jallcom.2024.178377
16. Zhu ZH, Zhang XZ, Niu JZ, Jia L, Liu N. Microstructure, texture and tensile properties of additive-manufactured Ti_2AlNb intermetallic fabricated by electron beam melting. *Int. J. Refract. Met. Hard Mater.* **2026**, *141*, 107993. DOI:10.1016/j.ijrmhm.2026.107993
17. Tang YJ, Zhao XH, Liu YT, Zhang YZ, Chen YQ. Microstructure and properties of laser additive manufacturing Ti_2AlNb-based alloy. *Heat Treat. Met.* **2016**, *41*, 1–6. DOI:10.13251/j.issn.0254-6051.2016.04.001
18. Zhang H, Zai L, Wang Y, Xue XH. Insight into microstructural evolution and mechanical property correlations of Ti_2AlNb-based alloy fabricated through wire arc additive manufacturing. *Mater. Sci. Eng. A* **2025**, *938*, 148477. DOI:10.1016/j.msea.2025.148477
19. Chen Q, Zhao L, Xu LY, Han YD. Fabricating Ti_2AlNb-based high temperature alloy via electron beam powder bed fusion. *Mater. Today Commun.* **2025**, *48*, 113682. DOI:10.1016/j.mtcomm.2025.113682
20. Zhang YQ, Xue KM, Meng M, Yan SL, Li P. High-temperature fracture behavior of Ti-22Al-26Nb with different featured microstructures. *Trans. Nonferrous Met. Soc. China* **2025**, *35*, 1155–1167. DOI:10.1016/S1003-6326(24)66740-3
21. Kang JM, Sun BB, Lu WQ, Qian M, Li JF. Cracking mechanisms in Ti_2AlNb alloy fabricated by laser powder bed fusion. *J. Alloys Compd.* **2025**, *1036*, 181979. DOI:10.1016/j.jallcom.2025.181979
22. Zhou M, Bu Z, Zhou Y, Wang J, Zhu L, Huang X, et al. The effect of primary and secondary O phase on the mechanical properties and deformation behavior of Ti_2AlNb alloy. *J. Alloys Compd.* **2025**, *1032*, 181160. DOI:10.1016/j.jallcom.2025.181160